Published in final edited form as:
Neuron. 2013 July 10; 79(1): 111–127. doi:10.1016/j.neuron.2013.04.029.

Modular use of peripheral input channels tunes motion-detecting circuitry

Marion Silies[1,#], **Daryl M. Gohl**[1,#], **Yvette E. Fisher**[1], **Limor Freifeld**[2], **Damon A. Clark**[1,3], and **Thomas R. Clandinin**[1,*]

[1]Department of Neurobiology, Stanford University, Stanford, CA 94305, USA

[2]Department of Electrical Engineering, Stanford University, Stanford, CA 94305, USA

SUMMARY

In the visual system, peripheral processing circuits are often tuned to specific stimulus features. How this selectivity arises and how these circuits are organized to inform specific visual behaviors is incompletely understood. Using forward genetics and quantitative behavioral studies, we uncover a new input channel to motion detecting circuitry in *Drosophila*. The second order neuron L3 acts combinatorially with two previously known inputs, L1 and L2, to inform circuits specialized to detect moving light and dark edges. *In vivo* calcium imaging of L3, combined with neuronal silencing experiments, suggests a neural mechanism to achieve selectivity for moving dark edges. We further demonstrate that different innate behaviors, turning and forward movement, can be independently modulated by visual motion. These two behaviors make use of different combinations of input channels. Such modular use of input channels to achieve feature extraction and behavioral specialization likely represents a general principle in sensory systems.

INTRODUCTION

Many animals have a diverse repertoire of innate behaviors that can be released by specific sensory stimuli (Tinbergen, 1951). To do this, the nervous system must extract relevant sensory cues from the environment and select the appropriate motor output. Visual cues such as form, color and motion guide a diverse array of essential behaviors. As information progresses inward from the periphery, neurons become tuned to increasingly complex visual features (Gollisch and Meister, 2010; Nassi and Callaway, 2009). However, how the early stages of feature-extraction in peripheral visual pathways are related to behavioral responses is poorly understood. We take advantage of a powerful genetic model, the fruit fly Drosophila, to define how inputs to motion processing circuits parse different signals into pathways that guide distinct motor outputs.

In the fruit fly, motion detection requires the synaptic outputs of a subset of photoreceptors, R1-R6 (Heisenberg, 1977; Wardill et al., 2012; Yamaguchi et al., 2008). R1-R6 project their axons into the first optic neuropil, the lamina, forming a retinotopic map of visual space (Figure 1A). This map comprises a reiterated array of 800 columnar elements. Within each

[*]Correspondence: trc@stanford.edu.
[#]these authors contributed equally to this work
[3]current address: Department of Cellular and Developmental Biology, Yale University, New Haven, CT 06511, USA

column, R1-R6 primarily make synaptic connections with three projection neurons, the lamina monopolar neurons L1, L2, and L3, as well as a local interneuron (amc), and glia (Figure 1B) (Meinertzhagen and O'Neil, 1991; Rivera-Alba et al., 2011). L1 and L2 were initially shown to be necessary and sufficient for motion vision, but to function largely redundantly, while L3 was thought to inform landmark orientation and spectral preference (Gao et al., 2008; Rister et al., 2007). More recent studies uncovered functional differences between the L1 and L2 channels, in that they provide inputs to pathways that are specialized for detecting moving edges of different contrast polarities. In particular, L1 provides input to a pathway that detects moving light edges, while L2 provides input to a pathway that detects moving dark edges (Clark et al., 2011; Joesch et al., 2010). The neural mechanisms by which these pathways become tuned to specific motion features remains controversial (Clark et al., 2011; Eichner et al., 2011; Reiff et al., 2010; Joesch et al., 2013). Much less is known about the neural circuits that lie downstream of this first synaptic relay. While L1-L3 represent all of the direct second order relays from R1-R6 photoreceptors into the next brain region, the medulla, L2 also makes synaptic contacts with a third order lamina monopolar cell, L4, which has been proposed to be important for motion detection based on its intriguing morphology (Braitenberg, 1970; Meinertzhagen and O'Neil, 1991 ; Strausfeld and Campos-Ortega, 1973, 1977; Takemura et al., 2011; Zhu et al., 2009). A fifth lamina monopolar cell, L5, receives few synaptic connections in the lamina, and has no known function.

Optomotor responses in Drosophila and other flies have largely been studied in flying animals (Borst et al., 2010; Götz, 1968; Heisenberg, 1979; Wolf, 1980). While many studies have focused on turning responses evoked by stimuli that rotate about the animal, other global motion patterns can also affect fly behavior, such as motion stimuli that would be associated with forward movement, pitch, or sideslip (Blondeau, 1982; Duistermars et al., 2012; Götz, 1968, 1973; Reiser and Dickinson, 2010; Tammero et al., 2004). In walking flies, motion signals can modulate both turning and forward movements (Götz, 1973; Hecht and Wald, 1934; Kalmus, 1949). Neuronal silencing experiments in freely walking flies suggested that some behavioral specialization for translational and rotational responses exists early in visual processing (Katsov and Clandinin, 2008). However, as freely walking flies experience complex visual stimuli, it remains unclear how neural circuits might precisely be specialized to respond to either translational or rotational signals.

In spite of this extensive analysis of motion vision in flies, central questions remain. What are the functional contributions of each of the input pathways from the lamina into the medulla? What are the neural mechanisms that underlie the differential tuning of motion detecting circuits for light and dark edges? How are inputs to motion detecting circuits specialized with respect to behavior? Using quantitative behavioral assays, *in vivo* calcium imaging and combinatorial genetic inactivation of the main input pathways to motion detection, we shed new light on these questions. We demonstrate that feature extraction and behavioral specialization use overlapping but distinct input channels in the peripheral visual system.

RESULTS

A forward genetic screen identifies L3 as a novel input for motion detection

While the lamina neurons L1 and L2 have been studied in detail, we sought to identify genetic tools to analyze the function of the two remaining critical relays in the lamina, L3 and L4. To do this, we performed a forward genetic screen using conditional neuronal inactivation. We established a collection of more than 1000 isogenic InSITE *Gal4* lines (Gohl et al., 2011). Gal4-mediated expression of a temperature sensitive *dynamin* allele (Kitamoto, 2001), *UAS-shibire*^{ts} (*UAS-shi*^{ts}) was used to inducibly inactivate defined

subsets of neurons immediately before testing. A phototaxis assay (S. Bhalerao and G. Dietzl, unpublished) was first used to exclude lines that displayed gross defects in movement (Figure 1C). Next, we used a population assay to quantify behavioral responses to motion (Katsov and Clandinin, 2008). Flies walking in glass tubes on a CRT monitor were shown brief presentations of two different random dot motion stimuli in which the dots were either lighter or darker than a gray background ("increment" and "decrement", Figure 1C). Using this paradigm, we screened 911 InSITE lines, and identified lines with behavioral deficits by comparing motion-evoked modulations of translational and rotational movements (Figure 1D–I). To quantify these changes, we used indices of translation and rotation, which capture changes in the fraction of flies that walk or turn at speeds above threshold values (Katsov and Clandinin, 2008). When rotation and translation indices were plotted against each other, cell types such as L1 and L2 that play critical roles in motion detection were clearly distinct from wild type controls (Figure 1D,E).

We then examined the expression patterns of lines with strong phenotypes, focusing on expression in lamina neurons, and phenotypes comparable to those associated with silencing L1 or L2. Silencing one line, *0595-Gal4*, differed significantly from both the *UAS-shi^{ts}/+* and *0595-Gal4/+* control for both motion-evoked modulations of rotation and translation behavior in response to the decrement stimulus (Figure 1D,F,G, Figure S1) and for rotation in response to the increment stimulus (Figure 1E,H,I, Figure S1). *0595-Gal4* specifically labeled the lamina neuron L3 in the optic lobe (Figure 2A,B). Single cell clones strongly labeled L3 cells, displaying a characteristic dendritic field that extended asymmetrically with respect to the primary neurite (Figure 2B). The axonal arbors of *0595-Gal4* expressing cells terminated in medulla layer M3 (Figure 2B, Figure S2; Fischbach and Dittrich, 1989). Moreover, this driver line, now designated *L3^{0595}-Gal4*, was highly specific in the visual system and weakly and stochastically labeled fewer than five other single medulla cells per brain and was expressed in fewer than 50 neurons in the central brain (Figure 2C). Together, these results suggested that L3 plays a role in motion processing.

Creating new genetic tools to specifically manipulate L4

L4 gets most of its synaptic inputs from L2 and is interconnected with neighboring dorso- and ventro-posterior cartridges (Meinertzhagen and O'Neil, 1991; Rivera-Alba et al., 2011; Takemura et al., 2011). This intriguing morphology led to proposals that L4 might provide input to a pathway specialized to detect progressive motion signals (Braitenberg, 1970; Rister et al., 2007; Takemura et al., 2011) and that L4 represents a critical component of motion detecting circuitry (Zhu et al., 2009). Based on expression analysis, we identified two independent L4-Gal4 lines, *L4^{0987}-Gal4* and *L4^{0980}-Gal4,* which surprisingly had only modest behavioral phenotypes (Figure 1D–I). These two lines had expression in a single class of lamina neurons with dendrites restricted to the proximal lamina, a characteristic feature of L4 (Figure 2D–I; Fischbach, 1989) and *L4^{0987}-Gal4* specifically labelled L4 in the visual system in single cell clones (Figure 2D,E, Figure S2). *L4^{0987}-Gal4* was also expressed in a small number of neurons in the subesophageal ganglion (SOG) (Figure 2F). *L4^{0980}-Gal4* was expressed in L4 and in a single class of medulla neurons, with additional sparse expression in the central brain (Figure 2G–I). The InSITE system allows enhancer trap expression patterns to be refined using intersectional approaches, or repurposed by replacement of *Gal4* with another genetic effector (Gohl et al., 2011). To specifically manipulate L4 function, we replaced the Gal4 drivers with either half of the split-*Gal4* system (Luan et al., 2006) and obtained a *splitL4-Gal4* line (*L4^{0980}-VP16AD, L4^{0987}-Gal4DBD*) that was expressed only in L4 and in no other neurons (Figure 2J–L). To generate tools that would allow independent manipulations of L4 and other cell types using different binary expression systems, we also replaced the *Gal4* in the L4 drivers with two other transcription factors, *LexA* and *QF* (Lai and Lee, 2006; Potter et al., 2010). The

L4^{0987-}LexA, *L4^{0987-}QF* and *L4^{0980-}QF* lines recapitulated the expression pattern of their *Gal4* progenitors (Figure 2M–O). *L4^{0987-}QF* was additionally expressed in trachea, which, however, did not interfere with our experiments.

L4 receives at least two sources of visual input

We first sought to determine the visual response properties of L4 (Figure 3A,B). We measured *in vivo* calcium signals from L4 terminals in medulla layers M2 and M4 (Figure 3B,C) using 2-photon-imaging of the genetically encoded calcium indicator *TN-XXL* (Figure 3D–G) (Mank et al., 2008; Reiff et al., 2010). When presented with alternating increases and decreases in light intensity, the average ratiometric calcium signal of all cells decreased when the light was on and increased when the light was off, in both layers M2 and M4 (Figure 3D and data not shown). This is consistent with L4 hyperpolarizing to brightening and depolarizing to darkening (Douglass and Strausfeld, 1995). Very similar calcium signals were seen when either *Gal4* or *QF* transcription factors were used to drive *TN-XXL* expression (Figure 3D, see Experimental Procedures).

Next we tested whether L4 displays direction-selective responses to motion. In response to a narrow bright bar, moving on a dark background at 10°/s, L4 terminals responded with an initial decrease in calcium signal associated with the light increment when the bar reached their receptive field, followed by an increase in calcium signal as the bar left the receptive field (Figure 3E). Using bars that moved either horizontally or vertically, we found no signs of direction-selectivity (Figure 3E). Similar results were obtained for bars moving at 20°/s and 50°/s (data not shown).

To characterize the response properties of L4 under continuous, dynamic stimulation, we used a rapidly flickering, uniform-field stimulus with gaussian distributed intensity changes. Using linear-filter estimation procedures, we extracted the temporal linear filter that best captured the calcium response as a function of time (Chichilnisky, 2001; Sakai et al., 1988). This linear filter had a large negative lobe consistent with a sign inversion of the input contrast (Figure S3), results that are similar to those previously described for L2 (Clark et al., 2011).

We next examined the anatomical and functional relationship between L4 and its potential pre-synaptic input L2. Using the *L4^{0987}-LexA* driver we first tested for GFP reconstitution across synaptic partners (GRASP) between L2 and L4 (Feinberg et al., 2008; Gordon and Scott, 2009). We detected reconstituted GFP signal in both the lamina and medulla, but this GFP signal was not restricted to areas where EM reconstructions had revealed direct synaptic connections between L2 and L4 (Figure S3; Takemura et al., 2011; Takemura et al., 2008). These GRASP signals likely reflect proximity of L2 and L4 processes, rather than synaptic contacts.

We next examined L4 calcium responses to light, while silencing either outer photoreceptors (R1-R6), or L2. When R1-R6 cells were specifically silenced, L4 responses were almost completely eliminated (Figure 3F). This demonstrates that the silencing protocol was effective and that, as expected, L4 responses depend strongly on inputs from R1-R6. Next, we silenced neuronal activity in L2. Remarkably, we detected no differences in L4 responses to light flashes, comparing L2-silenced animals with the control condition (Figure 3G). In addition, we could not detect any changes in response to moving bars, or to the gaussian flicker stimulus (data not shown). Notably, L2 silencing using an identical protocol revealed significant differences in electrophysiological recordings from neurons in the lobula plate, arguing that this protocol strongly disrupts L2 activity (Joesch et al., 2010). Thus, L4 gets additional functional inputs.

L3 responds to both contrast changes and moving bar stimuli

Given the strong phenotype of L3 silenced flies in the behavioral screen, we determined the visual response properties of L3 using *in vivo* imaging of calcium signals in L3 axon terminals (Figure 4A). When presented with flashes of light lasting two seconds, the calcium indicator ratio in L3 terminals decreased for contrast increments (brightening) and increased for contrast decrements (darkening) (Figure 4B) when averaged across all cells. When we selected responding cells using cross-correlation analysis, the response of all cells that were highly correlated with their mean (201/295, 68.1%) was indistinguishable in shape from the averaged trace for all cells, but slightly increased in response magnitude. In addition, responses in a small number of cells (40/295, 13.6%) were negatively correlated with the mean of all cells, and displayed increasing indicator ratios for brightening, and decreasing ratios for darkening (Figure S4). Such inverted responses are consistent with previous studies of L2 (Reiff et al., 2010; LF, DAC and TRC, unpublished). The remaining cells displayed no strong cross-correlation with the mean and had broadly weak responses (54/295, 18.3%, data not shown). Using the bar stimulus moving at 10°/s, L3 neurons responded to moving bars with an initial hyperpolarization, followed by a depolarization. This response shape was identical for a bar moving from left to right versus right to left or upward versus downward (Figure 4C). Thus, direction-selectivity must arise in downstream circuitry.

L3 displays sustained, asymmetric responses to contrast

To measure L3 responses to changes in light intensity under dynamic, continuous illumination we used the gaussian flicker stimulus and described L3 responses using a linear-nonlinear (LN) model. This model consists of a linear filter and a static nonlinearity. The linear filter represents the temporal sensitivity of the neuron, while the nonlinearity captures other aspects of the cell's response such as gain, threshold, and saturation (Figure 4D; Chichilnisky, 2001; Clark et al., 2011; Sakai et al., 1988). These studies revealed that the linear filter of L3 displayed a single lobe of negative polarity (Figure 4D). The neurotransmitter receptor that detects photoreceptor responses in arthropods is a histamine gated chloride channel. Thus, this inversion reflects the sign inverting synapse between photoreceptors and L3. Consistently, L3 displayed an increase in intracellular calcium to contrast decrements and a decrease in calcium to contrast increments. Interestingly, the temporal characteristics of the L3 linear filter were qualitatively different from those measured in L1, L2 and L4 (Figure 4D, Clark et al., 2011). In particular, while the initial response lobes of the linear filters for L1, L2 and L4 all decayed rapidly, reaching baseline in less than 400 ms, the L3 filter took almost three times as long to decay to baseline. These results demonstrate that stimulus features that happened hundreds of milliseconds in the past contributed to the calcium signal in L3 (Figure 4D). Interestingly, the static nonlinearity revealed that the mean calcium signal of L3 had different gains for increases and decreases in luminance (Figure 4D, Figure S4). This form was well fit by two linear functions, one for response increments (R^2 = 93.4) and one for response decrements (R^2 = 94.8), with a higher slope for the latter (Figure S4). The full LN model matched the response of the cells more closely than the linear prediction (R^2=0.67 and R^2=0.63, Figure 4E), mainly improving predictions for strong calcium responses (Figure 4E, arrowheads). The rectified properties of L3 were also apparent when the 200 ms delayed response to a given contrast was plotted (Figure S4). Thus, unlike L1, L2 and L4, which respond with similar gains to contrast increments and decrements, L3 is rectified and has a higher gain for contrast decrements. These physiological data suggest that L3 could be preferentially involved in dark edge motion detection.

L3 and L4 are individually dispensable for turning responses to motion

Given the intriguing physiological responses of L3 and the previously proposed role for L4 in motion detection, we tested the effect of silencing these neurons on behavioral responses in a single-fly-assay. We measured behavioral responses of tethered flies walking on an air-cushioned ball, surrounded by three visual stimulus displays, which allowed tight control of the visual stimulus presentation (Figure S5, Buchner, 1976; Clark et al., 2011). In this experimental paradigm, the movement of the animal's legs spins the ball, providing a quantitative measure of the turning and forward movement of the animal.

We examined the turning response of flies using an array of motion stimuli rotating about the animal (Figure 5). L1 and L2 are required redundantly for responses to rotating gratings (Clark et al., 2011; Rister et al., 2007; Joesch et al., 2010). Flies lacking L1 function have specific deficits in turning responses to rotating light edges (a transition from darker to brighter), while flies lacking L2 function have strong deficits in turning to moving dark edges (a transition from brighter to darker) (Figure 5A,B,D,E, S5, compare blue traces to both control traces; Clark et al., 2011). These results were substantiated by an opposing edge stimulus, in which light and dark edges move in opposite directions, which evokes little turning response in wild type flies, as the motion circuits tuned to light and dark edges cancel one another. L1-silenced flies turn in the direction of the dark edge motion (as the motion circuitry that normally responds to moving light edges is inactivated), whereas L2-silenced flies turn with the direction of light edge motion (as the motion circuitry that normally responds to moving dark edges is inactivated) (Figure S5; Clark et al., 2011). We next tested the behavioral contribution of L3 to motion detection. When we silenced L3 neurons using the *L3^{0595}-Gal4* line, we detected no significant deficits when presented with rotating square wave gratings, single edges of either polarity, or opposing edges (Figure 5G–I, blue traces, Figure S5). Likewise, flies in which the highly specific *splitL4-Gal4* line was used to silence L4, also responded nearly normally to rotational stimuli (Figure 5J–L, Figure S5). Similar results were obtained using the *L4^{0987}-Gal4* driver (Figure S5). Thus, neither L3 nor L4 are individually required to guide turning responses to rotational visual motion under the conditions tested.

Three lamina monopolar cell inputs provide input to dark edge motion detection

We next examined whether these single cell type inactivation experiments might mask redundant functions among input pathways. Interestingly, although L2-silencing alone reduced responses to rotating dark edges, and caused turning in the direction of light edge motion in an opposing edges stimulus, some dark edge response remained (Figure 5E). Since L3's physiological properties make it preferentially sensitive to contrast decrements, we tested whether L3 acts redundantly with L2. When both L2 and L3 were silenced, flies displayed turning responses to light edges (Figure 6A). However, they displayed no turning at all in response to a rotating dark edge stimulus, and turned more strongly in the direction of light edge motion in an opposing edge stimulus than flies in which L2 was silenced alone (Figure 6B,C, Figure S6). Thus, double silencing experiments uncovered a redundant role for L3 in the detection of moving dark edges.

As previously reported, L1 silenced flies are virtually non-responsive to moving light edges (Figure 5A) and flies in which both L1 and L2 are silenced do not respond to rotational stimuli (Figure 6D–F; Clark et al., 2011; Joesch et al., 2010; Rister et al., 2007). Given the residual dark edge response observed when L2 is silenced, this latter result is puzzling, as one would expect flies in which both L1 and L2 are silenced to display residual turning in response to dark edges (Figure 5E, 6E). One possible explanation for this synergy between L1 and L2 is that L1 might play a role in dark edge detection (in addition to its prominent role in light edge detection). To vigorously test this hypothesis, we silenced L1 and L3

simultaneously. While neither of these lines displayed any deficits in dark edge detection when silenced individually, surprisingly, when L1 and L3 were silenced together, they displayed little response to dark edge motion (Figure 6H). Thus, silencing L1 and L3 together produces deficits in dark edge detection indistinguishable from those observed when silencing L2, the previously proposed sole input to dark edge detection (Clark et al., 2011; Joesch et al., 2010; Eichner et al., 2011; Joesch et al., 2013). In addition, these flies were largely unable to respond to rotating square wave gratings containing both edge types (Figure 6I), and thus displayed a similarly strong phenotype to flies in which both L1 and L2 were silenced. In contrast, silencing L4 in combination with either L1, L2 or L3 did not enhance any of the phenotypes for silencing either lamina neuron on its own (Figure 6J–R, Figure S6), arguing that L4 does not function redundantly in motion detection under the conditions tested.

Taken together, these genetic interaction experiments expand the previous view of the input channels to motion detecting circuitry. In particular, behavioral responses to rotating light edges require only input from L1, whereas behavioral responses to rotating dark edges require L2 as well as redundant input from either L1 or L3.

Visual motion can independently modulate forward walking and turning

In addition to specialization for motion signals with different contrast polarities, behavioral specialization for turning and forward walking responses to visual motion were proposed to exist early in visual processing (Katsov and Clandinin, 2008). To map the various input channels to motion detecting circuits onto this behavioral specialization, we examined whether visual motion cues can modulate forward movements independent of turning. In the absence of a visual motion stimulus, flies, on average, moved forward and could turn in either direction. A visual motion stimulus in which square-wave gratings translated symmetrically past the animal, either progressively (from front to back) or regressively (from back to front) on both eyes, caused wild-type flies to slow their forward movement (Figure 7, S7). Such stimuli also contain singularities where the square wave gratings meet in front of the animal, producing a pole of expansion (for front-to-back movement) or convergence (for back-to-front movement). The expansion pole associated with front-to-back movement of the stimulus evoked strong turning responses, a phenomenon described as expansion avoidance (Figure S7; Reiser and Dickinson, 2010; Tammero et al., 2004). In addition, we found that flies modulated their forward movement in response to the appearance of static square wave contrast patterns, an apparent startle response (Figure 7B,D). We therefore constructed a stimulus in which a flickering 10° wide stripe of mean gray contrast masked the singularity. To uncouple the startle response from responses to motion, we interposed a 500 ms delay between the appearance of the pattern and the onset of its movement (Figure 7A). When wild-type flies were presented with this new stimulus, they slowed down with the appearance of the stationary square wave grating, recovered to baseline within less than 500 ms, and then strongly reduced their forward walking speed in response to both front-to-back and back-to-front motion (Figure 7B,F,H). This effect was observed in responses of each individual fly, regardless of its forward walking speed prior to motion onset (Figure 7C). In all subsequent plots, we therefore normalized each fly's response to the population mean forward walking speed in a 100 ms time interval prior to motion onset (Figure 7E–H). When flies were presented a no-motion control including the central stripe and static square wave grating, we observed only modest startle at stimulus onset and offset (Figure 7D). Importantly, presentation of a full field flicker at the same contrast frequency as the moving square wave grating, elicited only a weak response, comparable in strength to that associated with the startle (Figure S7). Moreover, this modulation of walking speed was independent of flicker frequency (Figure S7). Strikingly, both front-to-back and back-to-front motion evoked similar slowing responses, but did not

affect turning (Figure 7E–H). As expected for a motion effect, the strength of these slowing responses varied systematically as a function of contrast frequency (Figure 7F′,H′). Thus, visual motion can specifically modulate forward movement of flies without affecting their turning.

L2 and L3 are individually required for modulation of forward movement

To test whether the same input channels transmit motion cues that guide behavioral responses to translational versus rotational motion, we blocked synaptic transmission in L1-L4 individually while presenting stimuli that specifically modulate forward movements. Flies in which L1 was silenced displayed normal responses to both front-to-back and back-to-front moving translational stimuli (Figure 8A,B, Figure S8). Similar results were obtained using a second *L1-Gal4* line (Figure S8). Intriguingly, flies in which L2 was silenced exhibited decreased responses to both front-to-back and back-to-front moving square wave gratings (Figure 8C,D, Figure S8). Flies in which L3 was silenced responded more weakly than the *UAS-shi^{ts}* control to front-to-back motion, but were indistinguishable from the Gal4/+ control (Figure 8E). However, when the stimulus was moving from back to front, these flies displayed reduced forward walking (Figure 8F), particularly at higher contrast frequencies. Finally, silencing synaptic transmission in L4 alone did not cause any deficits in behavioral responses to translational motion (Figure 8G,H). Importantly, using these reagents to silence L4 did cause defects in behavioral responses to visual stimuli that did not contain motion cues. L4-silenced flies had a diminished startle response to the appearance of the bars in no-motion control stimuli (Figure S8), suggesting that L4 mediates transient responses to the appearance of static contrast patterns. Moreover, when there was no delay between the appearance of the bars and the onset of their movement, L4-silenced flies modulated their forward walking speed less than control flies (Figure 8I,J). This phenotype disappeared when appearance of the bars and motion were uncoupled. Thus, L4 function is not required for motion-evoked behavioral responses under the wide range of conditions tested. In summary, responses to translational motion are sensitive to manipulations of the specific individual input channels L2 and L3.

Responses to translational and rotational motion utilize different input architectures

Given the synergetic interactions between input channels for behavioral responses to rotational motion, we silenced L1-L4 in all possible pairwise combinations. Surprisingly, simultaneous silencing of both L1 and L2 did not enhance the L2 phenotype observed when flies were tested with translational motion cues moving in either direction (Figure 9A,B), contrasting the synergy previously observed for rotational stimuli (Clark et al., 2011; Joesch et al., 2010; Rister et al., 2007, Figure 6D–F). In addition, unlike the striking deficits in turning responses to rotational motion seen in flies in which L1 and L3 were simultaneously silenced, L1 did not enhance the effect of silencing L3 when using translational motion stimuli (Figure 9C,D). Finally, silencing L4 in combination with L1, L2 or L3 did not reveal any synergetic interactions (Figure S9).

These data raised the possibility that L2 and L3 together might provide all of the inputs to behavioral responses to translational motion. To test this idea, we simultaneously silenced both cells. Such animals displayed very little modulation of forward walking speed in response to front-to-back motion and no detectable slowing in response to back-to-front motion (Figure 9E,F, blue traces). These latter results were statistically indistinguishable from those obtained when outer photoreceptors were silenced (Figure 9G,H), arguing that L2 and L3 likely represent all the inputs that guide responses to translational motion. Thus, the circuits that guide responses to translational versus rotational motion utilize different input architectures (Figure 9I).

DISCUSSION

Detecting moving dark edges requires multiple lamina inputs

Previous work demonstrated that L1 and L2 provide inputs that are specialized for the detection of moving light and dark edges, respectively (Clark et al., 2011; Joesch et al., 2010). Here we demonstrate that a third input channel provides critical input to motion detection circuitry. While our data corroborate the view that L1 provides input to a pathway that can detect moving light edges, we show that the detection of moving dark edges utilizes three input channels. In particular, silencing both L1 and L3 produces animals that are virtually blind to rotational motion, demonstrating that L2 inputs alone are insufficient to drive dark edge motion detection (Figure 6). Moreover, silencing either L1 or L3 in combination with L2 produces a stronger deficit in detecting rotating dark edges than silencing L2 alone. Thus, in addition to L2, dark edge motion detection also requires inputs from L1 and L3.

These conclusions differ from those obtained when L2 was tested in a sufficiency experiment that rescued motion detection through cell-type specific expression of a rescue transgene for the *outer rhabdomeres transientless (ort)* gene, which encodes a histamine gated chloride channel (Gengs et al., 2002; Joesch et al., 2010; Rister et al., 2007). However, these sufficiency experiments were performed using a hypomorphic allele, ort^{US2515} in *trans* to a null allele. ort^{US2515} has no changes in the *ort* coding sequence and unaltered transcript levels (Gengs et al., 2002). Thus, this allele presumably affects *ort* regulatory sequences, raising the possibility that it might not affect all cells equally. Indeed, the *ort* mutant background used in these experiments also retains significant vision (Gao et al., 2008; Rister et al., 2007). Thus, the discrepancy between these previous studies and our present work could be explained by residual expression of Ort protein in either L1 or L3 in the original rescue experiments. Thus, while Rister et al. (2008) originally identified L1 and L2 as the two main inputs driving turning behavior, and more specialized stimuli could subsequently assign them to light and dark edge pathways (Clark et al., 2011; Joesch et al., 2010), we now uncover new contributors to the dark edge pathway that were previously masked.

L4 function is not required for motion detection under many conditions

Because motion detection requires comparing signals from two points in space, connections between columnar inputs representing information collected from neighboring points in visual space are required. L4, which receives its main input from L2, sends collateral projections to neighboring dorso-posterior and ventro-posterior cartridges, where it provides input both to L2 and L4 cells (Meinertzhagen and O'Neil, 1991; Rivera-Alba et al., 2011). This striking connectivity pattern has inspired several models for L4 function, including the hypothesis that L4 functions in lateral interactions (Strausfeld and Campos-Ortega, 1973, 1977), that L4 acts as the interconnection between elementary motion detector arrays (Braitenberg, 1970; Zhu et al., 2009), or that L4 is specialized to detect front-to-back motion (Rister et al., 2007; Takemura et al., 2011; Takemura et al., 2008). We have shown that L4 must get functionally significant inputs from cells other than L2 (Figure 3). Such inputs could be provided directly by photoreceptors, or via the interneuron amc (Meinertzhagen and O'Neil, 1991; Rivera-Alba et al., 2011), but require a sign inverting synapse between photoreceptors and L4. Although predictions of connectivity based on anatomy will be tremendously helpful, our analysis of the L2-L4 link sounds a cautionary note regarding the importance of functional validation for these connections.

Using novel genetic reagents restricted to L4, we saw no effect of silencing L4 on behavioral responses to translational motion or rotational motion cues (Figures 5,6,8,9). Finally, we detected a role for L4 in the startle response caused by the appearance of static

contrast patterns (Figure 8). Thus, our results argue that L4 does not have a specific role in motion detection, though it is possible that L4 provides input to motion detecting circuits under stimulus conditions outside the range we have explored. These results contrast with a previous behavioral study that proposed a central role for L4 in motion vision based on a driver line that was expressed strongly in L3 and L4, as well as weakly in L2 and L5 (Zhu et al., 2009). Given that L3 functions in motion detection, it is likely that the phenotypes observed in this previous work can be attributed to the effects of inactivating L3, in combination with other lamina neurons. Finally, we note that the pattern of connections made by L4 is also consistent with a role for L4 in spatial summation (Rister et al., 2007; Takemura et al., 2011). In this view, L4 serves to pool information about local contrast changes.

L3 displays sustained, asymmetric responses to contrast

Two very different mechanisms by which motion detecting pathways could be made selective for light or dark edges have been proposed. In one view, the L1 and L2 inputs into motion detectors are independently half-wave rectified such that each pathway predominantly transmits information about only contrast increments or contrast decrements, as well as a weaker signal proportional to the average intensity of light (Eichner et al., 2011; Joesch et al., 2010; Reiff et al., 2010; Joesch et al., 2013). Alternatively, edge contrast selectivity can also be achieved through the incorporation of differential weighting of computations that detect specific correlations in the stimulus (Clark et al., 2011). Here, the motion detectors downstream of both L1 and L2 must receive information about both contrast increments and decrements. While calcium imaging experiments using large contrast steps argued that L2 is half-wave rectified (Reiff et al., 2010), a subsequent study using dynamic stimuli demonstrated that L2 is sensitive to both contrast increments and decrements (Clark et al., 2011). Using a dynamic gaussian noise stimulus, we demonstrate that L3's responses to contrast changes are non-linear, displaying a higher gain for contrast decrements than increments (Figure 4). As our genetic experiments demonstrate that L3 makes a critical contribution to dark edge motion detection, pre-synaptic rectification indeed occurs in one of the input channels to motion detection circuits that respond selectively to dark edge motion. Moreover, by having one channel, L2, that is sensitive to both contrast increments and decrements, and a second channel, L3, that predominantly transmits information about contrast decrements, dark edge selectivity could incorporate both previously proposed tuning mechanisms.

In addition to L3's non-linear properties, calcium signals in the L3 synaptic terminal are longer lasting than those in other lamina neurons. These protracted kinetics shed light on a long-standing observation regarding the neural mechanisms of motion detection. Unlike our measurements of the calcium signals in L1, L2 and L4, where the linear filters decay rapidly, L3's linear filter takes almost three times as long to decay. Since the stimulus, the analysis procedure, and the expression of the calcium indicator were similar to experiments where sharp, derivative-taking filters were estimated, this extended response is unlikely the product of measurement artifacts, or indicator properties. Thus, these results suggest that L3 terminals present sustained responses, preserving information about contrast changes for relatively long periods of time.

Many lines of evidence demonstrate that contrast provides critical input to the Hassenstein-Reichardt Correlator (HRC), the computational model that describes many aspects of motion vision (Borst et al., 2010; Hassenstein, 1956). However, both behavioral and electrophysiological evidence demonstrates that motion signals can be produced from sequential illumination of two neighboring points in space, even when the second point of illumination is significantly delayed relative to the first (Clark et al., 2011; Egelhaaf and Borst, 1992; Eichner et al., 2011). This suggested that information about luminance, rather

than contrast, are incorporated, creating a “DC” signal (Eichner et al., 2011). We speculate that the long time constant observed in the temporal linear filtering properties of L3 contributes to these phenomena.

Behavioral specialization in motion detecting circuits

Motion cues guide many different innate behavioral responses in fruit flies, with subtly different cues sometimes eliciting dramatically different behavioral responses (Maimon, 2008). Motion induces responses that affect displacements of the animal’s body along various axes of movement (including, for example, yaw, pitch and slip), as well as rotations of the animal’s head (Blondeau, 1982; Duistermars et al., 2007; Götz, 1968, 1973; Rister et al., 2007; Tammero et al., 2004; Theobald et al., 2010). Some of these behavioral responses display distinct tuning properties (Duistermars et al., 2007; Tammero et al., 2004; Theobald et al., 2010). Work in other arthropods demonstrates that translational and rotational cues can be independently analyzed to inform distinct behaviors (Collett, 1980; Junger and Dahmen, 1991; Barnes 1990). Previous work comparing turning and forward movements in freely walking flies proposed that these two behavioral responses were the products of specialized neural circuits that diverge early in the visual system (Katsov and Clandinin, 2008). However, in this previous study, flies experienced complex patterns of optic flow comprising both rotational and translational components, making the extent of this separation unclear. We established a behavioral paradigm in which single walking flies modulated their forward walking speed in response to motion signals without changing their turning, thereby uncoupling these two behavioral responses (Figure 7). Combining this paradigm with specific neuronal manipulations of input channels, both individually and in combination, we demonstrate that L1, L2 and L3 are required for motion detection, but are individually specialized (Figure 9I). One of these cells, L1, only provides input to motion detectors that guide turning. L2 and L3, on the other hand, provide input both to detectors that guide turning as well as forward walking. Thus, the input pathways that couple turning and forward walking to motion are different.

Modular peripheral inputs guide behavior

Our data demonstrate that distinct but overlapping combinations of inputs to motion detecting circuits are tuned to particular stimulus features and linked to specific behavioral outputs (Figure 9I). First, light edge detecting circuits require inputs from L1, while dark edge detecting circuits utilize inputs from L1, L2, and L3. Second, the ability of motion signals to modulate turning responses requires inputs from L1, L2 and L3 (Figures 5, 6), while the modulation of forward walking speed requires only the inputs of L2 and L3 (Figure 8, 9). As our data demonstrate, overlapping sets of neurons, each with different physiological properties and connections, are combined into modules that inform different behavioral outputs. Such a combinatorial use of input channels represents an efficient way to generate a variety of coding possibilities using a limited set of neurons. Given that L1, L2 and L3 make a diverse array of synaptic contacts in the medulla, our data also raise the possibility that downstream motion computations are distributed amongst many different neuron types. Specific subsets of these downstream pathways could then converge in deeper layers of the visual system to tune neurons to particular motion features (de Vries and Clandinin, 2012; Egelhaaf et al., 2002; Hausen, 1982; Krapp et al., 1998; Mu et al., 2012). These more specialized neurons could then inform specific motor outputs appropriate to the visual stimulus. It will be interesting to investigate if distinct input modules control motion induced behaviors in, for example, flying or freely walking flies.

Given the anatomical parallels between vertebrate and invertebrate visual systems (Sanes and Zipursky, 2010), our studies suggest that the early extraction of features through combinatorial use of input channels may result in specialized behavioral outcomes in other

systems. Thus, while different stimulus features can be processed in parallel in the fly and vertebrate visual systems, our results highlight the importance of understanding how these parallel pathways are interwoven to modulate behavioral outcome. Such modular use of peripheral input pathways likely represents a general strategy for coupling particular combinations of stimulus features to specific motor outputs in many sensory systems.

EXPERIMENTAL PROCEDURES

Fly stocks

Driver Lines: The following *Gal4* lines were used to direct cell-specific expression: *Rh1-Gal4* (Bloomington Drosophila Stock Center, BDSC), *L1a-Gal4* (*vGlut-dVP16AD, ortC2-GAL4DBD*) (Gao et al., 2008), *L1b-Gal4* (*c202-GAL4*) and *L2-Gal4* (*21DGal4*) (Rister et al., 2007). In addition, the following InSITE *Gal4* lines and swaps were generated in this study: $L3^{0595}$*-Gal4* (*PBac{IT.GAL4}0595*), $L4^{0980}$*-Gal4* (*PBac{IT.GAL4}0980*), $L4^{0987}$*-Gal4* (*PBac{IT.GAL4}0987*), $L4^{0980}$*-VP16AD* (*PBac{IS.VP16AD.w-}0980*), $L4^{0987}$*-Gal4DBD* (*PBac{IS.Gal4DBD.w-}0987*), *splitL4-Gal4* ($L4^{0980}$*-VP16AD;* $L4^{0987}$*-Gal4DBD*), $L4^{0987}$*-LexA* (*PBac{IS.LexA.w-}0987*), $L4^{0980}$*-QF* (*PBac{IS.QF.w-}0980*), $L4^{0987}$*-QF* (*PBac{IS.QF.w-}0987*).

Effector lines: *UAS-TN-XXL* ((Mank et al., 2008), local hops generated by Clark et al. (2011)), *QUAS-TN-XXL* (this study), *LexAop-CD4::spGFP11*, *UAS-CD4::spGFP1-10* (Gordon and Scott, 2009), *UAS-*^{myr}*tdTomato*, *UAS-mCD8::GFP, UAS-shi*^{ts} (BDSC), *UAS>CD2,y*$^{+}$*>mCD8::GFP* (Wong et al., 2002). While backcrossing *UAS-shi*^{ts} (on chromosome III), at least two independent transgenes were detected. These were backcrossed individually and then recombined onto a single chromosome. InSITE enhancer trap lines were generated by mobilizing one of two starting *piggyBac* elements, *PBac{IT.Gal4}1.1*, or *PBac{IT.GAL4}0315* (Gohl, 2011), or by micro-injection (Rainbow Transgenic Flies, Inc., Camarillo, CA). The *piggyBac* transposase stocks *J2 (Her{3xP3-ECFP, atub-piggyBac-K10}M2)* (Hacker et al., 2003), and *CyO, P{Tub-PBac|T}2* (BDSC) (Thibault et al., 2004) were used for mobilization.

In order to minimize strain effects, all constructs used for behavior were backcrossed five times into an isogenized OregonR background. All InSITE lines and swaps were generated in this isogenic background. InSITE *Gal4* lines were genetically swapped to other effectors and confirmed by PCR as previously described (Gohl, 2011).

Behavioral experiments

Population behavioral experiments were done as in Katsov and Clandinin (2008), using sparse (20% density) random dot stimuli comprising contrast increments or decrements. Behavioral experiments with tethered flies walking on an air-suspended ball were essentially done as in Clark et al. (2011). The stimulus display was modified and stimuli were projected onto rear-projection screens surrounding the fly. Flies were shown different rotation stimuli (rotating square wave gratings, single dark and light edges, opposing edges) or a translational stimulus moving either front-to-back or back-to-front. Female flies of all genotypes were tested at 34°C, a restrictive temperature for Shi^{ts} activity.

Calcium imaging experiments

In vivo calcium imaging was done largely as described in Clark et al. (2011). The stimulus display was modified and stimuli were projected onto a rear-projection screen in front of the fly. Flies were shown 2 s-lasting full field light flashes, a moving bar or a gaussian random flicker stimulus.

See Supplemental Experimental Procedures for detailed methods.

Supplementary Material

Refer to Web version on PubMed Central for supplementary material.

Acknowledgments

We thank Nirao Shah, Liqun Luo, Christian Klämbt, David Kastner, Girish Deshpande, Saskia de Vries, Jennifer Esch, and Tina Schwabe for critical comments on the manuscript. We thank Georg Dietzl and Sheetal Bhalerao for providing the phototaxis assay, Christoph Scheper and Ya-Hui Chou for brain dissections and Alexander Katsov for help with the high-throughput behavioral assay. M.S. and D.A.C. acknowledge postdoctoral fellowship from the Jane Coffin Childs Memorial Fund for Medical Research. D.M.G was supported by a Ruth L. Kirschstein NRSA Postdoctoral Fellowship (F32EY020040) from the National Eye Institute. Y.E.F. acknowledges an NIH Neuroscience Research Training grant (5 T32 MH020016-14) and L.F. was supported by a Fulbright International Science and Technology Scholarship and a Bio-X Stanford Interdisciplinary Graduate Fellowship (Bruce and Elizabeth Dunlevie fellow). D.A.C also received support from an NIH T32 Postdoctoral Training Grant. This work was funded by a National Institutes of Health Director's Pioneer Award DP1 OD003530 (T.R.C.) and by R01 EY022638.

References

Barnes JP. Sensory basis and functional role of eye movements elicited during locomotion in the land crab *Cardisoma guanhumi*. J Exp Biol. 1990; 154:99–119.

Blondeau J. Electrically evoked course control in the fly *Calliphora erythrocephala*. J Exp Biol. 1981; 92:143–153.

Blondeau J, Heisenberg M. The three-dimensional optomotor torque system of Drosophila melanogaster. J Comp Physiol A. 1982; 145:321–329.

Borst A, Haag J, Reiff DF. Fly motion vision. Annu Rev Neurosci. 2010; 33:49–70. [PubMed: 20225934]

Braitenberg V. Order and orientation of elements in the visual system of the fly. Kybernetik. 1970; 7:235–242. [PubMed: 4324777] High-throughput ethomics in large groups of Drosophila. Nat Methods. 6:451–457.

Buchner E. Elementary Movement Detectors in an Insect Visual System. Biol Cybernetics. 1976; 24:85–101.

Chiappe ME, Seelig JD, Reiser MB, Jayaraman V. Walking modulates speed sensitivity in Drosophila motion vision. Curr Biol. 2010; 20:1470–1475. [PubMed: 20655222]

Chichilnisky EJ. A simple white noise analysis of neuronal light responses. Network. 2001; 12:199–213. [PubMed: 11405422]

Clark DA, Bursztyn L, Horowitz MA, Schnitzer MJ, Clandinin TR. Defining the computational structure of the motion detector in Drosophila. Neuron. 2011; 70:1165–1177. [PubMed: 21689602]

Collett TS. Some operating rules for the optomotor system of a hoverfly during voluntary flight. J Comp Physiol. 1980; 138:271–282.

de Vries SE, Clandinin TR. Loom-sensitive neurons link computation to action in the Drosophila visual system. Curr Biol. 2012; 22:353–362. [PubMed: 22305754]

Douglass JK, Strausfeld NJ. Visual motion detection circuits in flies: peripheral motion computation by identified small-field retinotopic neurons. J Neurosci. 1995; 15:5596–5611. [PubMed: 7643204]

Douglass JK, Strausfeld NJ. Visual motion detection circuits in flies: parallel direction-selective and non-direction-selective pathways between the medulla and the lobula plate. J Neurosci. 1996; 16:4551–4562. [PubMed: 8764644]

Duistermars BJ, Care RA, Frye MA. Binocular interactions underlying the classic optomotor responses of flying flies. Front Behav Neurosci. 2012; 6:6. [PubMed: 22375108]

Duistermars BJ, Chow DM, Condro M, Frye MA. The spatial, temporal and contrast properties of expansion and rotation flight optomotor responses in Drosophila. J Exp Biol. 2007; 210:3218–3227. [PubMed: 17766299]

Egelhaaf M, Borst A. Are there separate ON and OFF channels in fly motion vision? Visual Neuroscience. 1992; 8:151–164. [PubMed: 1558827]

Egelhaaf M, Borst A, Reichardt W. Computational structure of a biological motion-detection system as revealed by local detector analysis in the fly's nervous system. J Opt Soc Am A. 1989; 6:1070–1087. [PubMed: 2760723]

Egelhaaf M, Kern R, Krapp HG, Kretzberg J, Kurtz R, Warzecha AK. Neural encoding of behaviourally relevant visual-motion information in the fly. Trends Neurosci. 2002; 25:96–102. [PubMed: 11814562]

Eichner H, Joesch M, Schnell B, Reiff DF, Borst A. Internal structure of the fly elementary motion detector. Neuron. 2011; 70:1155–1164. [PubMed: 21689601]

Feinberg EH, Vanhoven MK, Bendesky A, Wang G, Fetter RD, Shen K, Bargmann CI. GFP Reconstitution Across Synaptic Partners (GRASP) defines cell contacts and synapses in living nervous systems. Neuron. 2008; 57:353–363. [PubMed: 18255029]

Fischbach KF, Dittrich APM. The optic lobe of *Drosophila melanogaster*. I. A Golgi analysis of wild-type structure. Cell Tissue Res. 1989; 258:441–475.

Gao S, Takemura SY, Ting CY, Huang S, Lu Z, Luan H, Rister J, Thum AS, Yang M, Hong ST, et al. The neural substrate of spectral preference in Drosophila. Neuron. 2008; 60:328–342. [PubMed: 18957224]

Gengs C, Leung HT, Skingsley DR, Iovchev MI, Yin Z, Semenov EP, Burg MG, Hardie RC, Pak WL. The target of Drosophila photoreceptor synaptic transmission is a histamine-gated chloride channel encoded by ort (hclA). J Biol Chem. 2002; 277:42113–42120. [PubMed: 12196539]

Gohl DM, Silies MA, Gao XJ, Bhalerao S, Luongo FJ, Lin CC, Potter CJ, Clandinin TR. A versatile in vivo system for directed dissection of gene expression patterns. Nature Methods. 2011; 8:231–237. [PubMed: 21473015]

Gollisch T, Meister M. Eye Smarter than Scientists Believed: Neural Computations in Circuits of the Retina. Neuron. 2010; 65:150–164. [PubMed: 20152123]

Gordon MD, Scott K. Motor control in a Drosophila taste circuit. Neuron. 2009; 61:373–384. [PubMed: 19217375]

Götz KG. Optomotorische Untersuchung des visuellen Systems einiger Augenmutanten der Fruchtfliege Drosophila. Kybernetik. 1964; 2:77–92. [PubMed: 5833196]

Götz KG. Flight control in Drosophila by visual perception of motion. Kybernetik. 1968; 4:199–208. [PubMed: 5731498]

Götz KG, Wenking H. Visual control of locomotion in the walking fruitfly Drosophila. J Comp Physiol A. 1973; 85:235–266.

Hacker U, Nystedt S, Barmchi MP, Horn C, Wimmer EA. piggyBac-based insertional mutagenesis in the presence of stably integrated P elements in Drosophila. Proc Natl Acad Sci U S A. 2003; 100:7720–7725. [PubMed: 12802016]

Hassenstein B, Reichardt W. Systemtheoretische Analyse der Zeit-, Reihenfolgen- und Vorzeichenauswertung bei der Bewegungsperzeption des Rüsselkäfers Chlorophanus. Zeitschrift für Naturforschung B. 1956; 11:513–524.

Hausen K. Motion sensitive interneurons in the optomotor system of the fly. II. The horizontal cells: receptive field organization and response characteristics. Biological Cybernetics. 1982; 46:67–79.

Hecht S, Wald G. The Visual Acuity and Intensity Discrimination of Drosophila. J Gen Physiol. 1934; 17:517–547. [PubMed: 19872798]

Heisenberg M, Wolf R. On the fine structure of yaw torque in visual flight orientation of Drosophila melanogaster. J Comp Physiol A. 1979; 130:113–130.

Heisenberg M, Buchner E. The role of retinula cell types in visual behavior of *Drosophila Melanogaster*. J Comp Physiol A. 1977; 187:127–162.

Joesch M, Schnell B, Raghu SV, Reiff DF, Borst A. ON and OFF pathways in Drosophila motion vision. Nature. 2010; 468:300–304. [PubMed: 21068841]

Joesch M, Weber F, Eichner H, Borst A. Functional specialization of parallel motion detection circuits in the fly. J Neurosc. 2013; 33:902–905.

Junger W, Dahmen HJ. Response to self-motion in waterstriders: visual discrimination between rotation and translation. J Comp Physiol A. 1991; 169:641–646.

Kalmus H. Optomotor responses in Drosophila and Musca. Physiol Comp Ocol Int J Comp Physiol Ecol. 1949; 1:127–147. [PubMed: 18118972]

Katsov AY, Clandinin TR. Motion processing streams in Drosophila are behaviorally specialized. Neuron. 2008; 59:322–335. [PubMed: 18667159]

Kitamoto T. Conditional modification of behavior in Drosophila by targeted expression of a temperature-sensitive shibire allele in defined neurons. J Neurobiol. 2001; 47:81–92. [PubMed: 11291099]

Krapp HG, Hengstenberg B, Hengstenberg R. Dendritic structure and receptive-field organization of optic flow processing interneurons in the fly. J Neurophysiol. 1998; 79:1902–1917. [PubMed: 9535957]

Lai SL, Lee T. Genetic mosaic with dual binary transcriptional systems in Drosophila. Nat Neurosci. 2006; 9:703–709. [PubMed: 16582903]

Lee CH, Herman T, Clandinin TR, Lee R, Zipursky SL. N-cadherin regulates target specificity in the Drosophila visual system. Neuron. 2001; 30:437–450. [PubMed: 11395005]

Luan H, Peabody NC, Vinson CR, White BH. Refined spatial manipulation of neuronal function by combinatorial restriction of transgene expression. Neuron. 2006; 52:425–436. [PubMed: 17088209]

Mank M, Santos AF, Direnberger S, Mrsic-Flogel TD, Hofer SB, Stein V, Hendel T, Reiff DF, Levelt C, Borst A, et al. A genetically encoded calcium indicator for chronic in vivo two-photon imaging. Nat Methods. 2008; 5:805–811. [PubMed: 19160515]

Meinertzhagen IA, O'Neil SD. Synaptic organization of columnar elements in the lamina of the wild type in Drosophila melanogaster. J Comp Neurol. 1991; 305:232–263. [PubMed: 1902848]

Mu L, Ito K, Bacon JP, Strausfeld NJ. Optic glomeruli and their inputs in Drosophila share an organizational ground pattern with the antennal lobes. J Neurosci. 2012; 32:6061–6071. [PubMed: 22553013]

Nassi JJ, Callaway EM. Parallel processing strategies of the primate visual system. Nat Rev Neurosci. 2009; 10:360–372. [PubMed: 19352403]

O'Carroll DC, Bidwell NJ, Laughlin SB, Warrant EJ. Insect motion detectors matched to visual ecology. Nature. 1996; 382:63–66. [PubMed: 21638927]

Potter CJ, Tasic B, Russler EV, Liang L, Luo L. The Q system: a repressible binary system for transgene expression, lineage tracing, and mosaic analysis. Cell. 2010; 141:536–548. [PubMed: 20434990]

Reiff DF, Plett J, Mank M, Griesbeck O, Borst A. Visualizing retinotopic half-wave rectified input to the motion detection circuitry of Drosophila. Nat Neurosci. 2010; 13:973–978. [PubMed: 20622873]

Reiser MB, Dickinson MH. Drosophila fly straight by fixating objects in the face of expanding optic flow. J Exp Biol. 2010; 213:1771–1781. [PubMed: 20435828]

Rister J, Pauls D, Schnell B, Ting CY, Lee CH, Sinakevitch I, Morante J, Strausfeld NJ, Ito K, Heisenberg M. Dissection of the peripheral motion channel in the visual system of Drosophila melanogaster. Neuron. 2007; 56:155–170. [PubMed: 17920022]

Rivera-Alba M, Vitaladevuni SN, Mischenko Y, Lu Z, Takemura SY, Scheffer L, Meinertzhagen IA, Chklovskii DB, de Polavieja GG. Wiring economy and volume exclusion determine neuronal placement in the Drosophila brain. Curr Biol. 2011; 21:2000–2005. [PubMed: 22119527]

Sakai HM, Naka K, Korenberg MJ. White-noise analysis in visual neuroscience. Vis Neurosci. 1988; 1:287–296. [PubMed: 3154801]

Salcedo E, Zheng L, Phistry M, Bagg EE, Britt SG. Molecular basis for ultraviolet vision in invertebrates. J Neurosci. 2003; 23:10873–10878. [PubMed: 14645481]

Sanes JR, Zipursky SL. Design principles of insect and vertebrate visual systems. Neuron. 2010; 66:15–36. [PubMed: 20399726]

Schnell B, Raghu SV, Nern A, Borst A. Columnar cells necessary for motion responses of wide-field visual interneurons in *Drosophila*. J Comp Physiol A. 2012; 198:389–395.

Strausfeld NJ, Campos-Ortega JA. The L4 monopolar neurone: a substrate for lateral interaction in the visual system of the fly Musca domestica (L.). Brain Res. 1973; 59:97–117. [PubMed: 4747774]

Strausfeld NJ, Campos-Ortega JA. Vision in insects: pathways possibly underlying neural adaptation and lateral inhibition. Science. 1977; 195:894–897. [PubMed: 841315]

Takemura SY, Karuppudurai T, Ting CY, Lu Z, Lee CH, Meinertzhagen IA. Cholinergic circuits integrate neighboring visual signals in a Drosophila motion detection pathway. Curr Biol. 2011; 21:2077–2084. [PubMed: 22137471]

Takemura SY, Lu Z, Meinertzhagen IA. Synaptic circuits of the Drosophila optic lobe: the input terminals to the medulla. J Comp Neurol. 2008; 509:493–513. [PubMed: 18537121]

Tammero LF, Frye MA, Dickinson MH. Spatial organization of visuomotor reflexes in Drosophila. J Exp Biol. 2004; 207:113–122. [PubMed: 14638838]

Theobald JC, Ringach DL, Frye MA. Dynamics of optomotor responses in Drosophila to perturbations in optic flow. J Exp Biol. 2010; 213:1366–1375. [PubMed: 20348349]

Thibault ST, Singer MA, Miyazaki WY, Milash B, Dompe NA, Singh CM, Buchholz R, Demsky M, Fawcett R, Francis-Lang HL, et al. A complementary transposon tool kit for Drosophila melanogaster using P and piggyBac. Nat Genet. 2004; 36:283–287. [PubMed: 14981521]

Tinbergen, N., editor. The Study of Instinct. London: Oxford University Press; 1951.

Wardill TJ, List O, Li X, Dongre S, McCulloch M, Ting CY, O'Kane CJ, Tang S, Lee CH, Hardie RC, et al. Multiple spectral inputs improve motion discrimination in the Drosophila visual system. Science. 2012; 336:925–931. [PubMed: 22605779]

Wolf R, Heisenberg M. On the fine structure of yaw torque in visual flight orientation of Drosophila melanogaster. J Comp Physiol A. 1980; 140:69–80.

Wong AM, Wang JW, Axel R. Spatial representation of the glomerular map in the Drosophila protocerebrum. Cell. 2002; 109:229–241. [PubMed: 12007409]

Yamaguchi S, Wolf R, Desplan C, Heisenberg M. Motion vision is independent of color in Drosophila. Proc Natl Acad Sci U S A. 2008; 105:4910–4915. [PubMed: 18353989]

Zhu Y, Nern A, Zipursky SL, Frye MA. Peripheral visual circuits functionally segregate motion and phototaxis behaviors in the fly. Curr Biol. 2009; 19:613–619. [PubMed: 19303299]

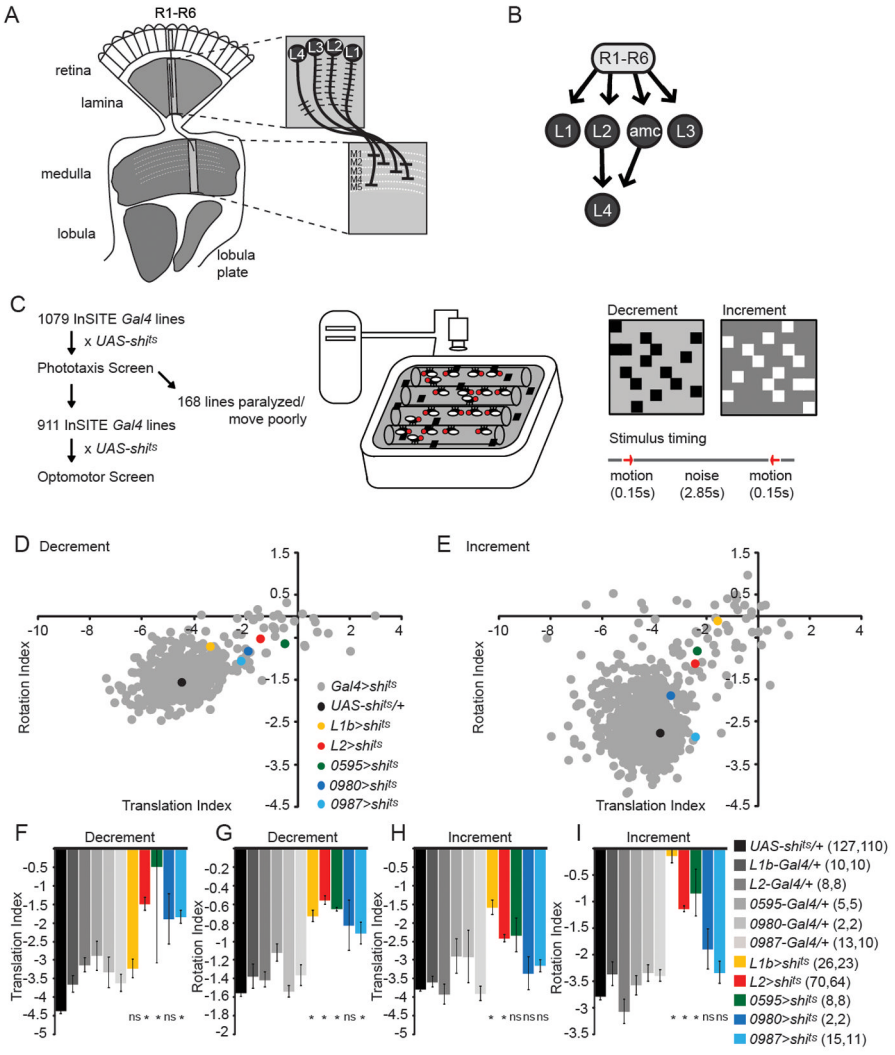

Figure 1. A forward genetic screen to identify neurons required for motion detection

(A) Schematic of the *Drosophila* visual system. One lamina cartridge and one medulla column are magnified to show the dendritic and axonal arborization patterns of the lamina neurons L1-L4. **(B)** Photoreceptors (R1-R6) make synaptic connections with L1, L2, L3 and the amc interneuron. L4 receives most inputs from L2 and amc. **(C)** Workflow for the behavioral screen and schematic illustration of the population optomotor assay, stimuli and trial structure. **(D, E)** Scatter plots of translation and rotation indices, summarizing screen results for decrement **(D)** and increment **(E)** stimuli. **(F–I)** Bar plots of translation and rotation indices for both decrement and increment stimuli. Genotypes as indicated. Number of tubes of flies run per genotype is given in parentheses for decrement stimulus and increment stimulus, respectively. *p<0.05, tested using two-tailed t-tests against both controls, ns = not significant, error bars denote +/− 1 standard error of the mean (SEM). See also Figure S1.

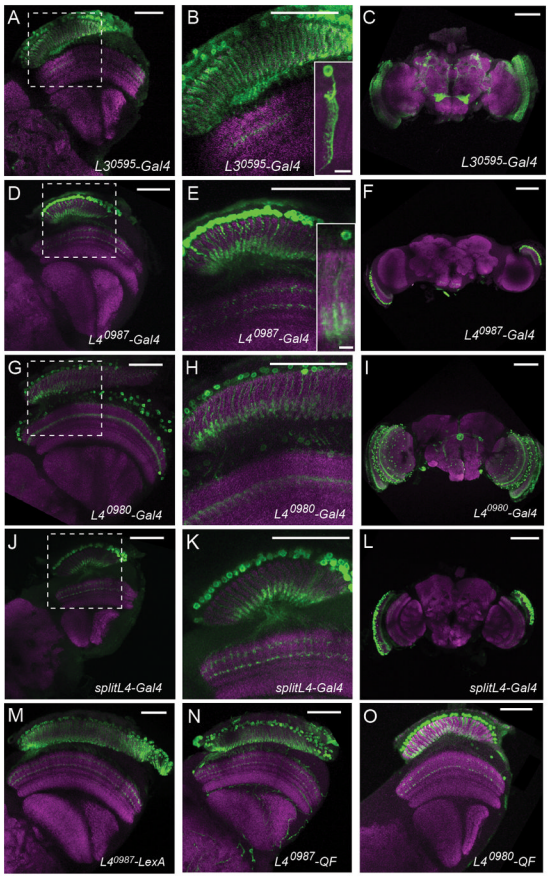

Figure 2. Expression patterns of the identified L3 and L4 lines

(A–O) Confocal images of adult brains stained with anti-GFP (green) and anti-Bruchpilot (nc82; magenta). **(A–C)** *L3^{0595}* driving *UAS-mCD8::GFP*. **(D–F)** *L4^{0987}-Gal4* driving *UAS-mCD8::GFP*. Insets in **(B,D)**: *L3^{0595}- /L4^{0987}-Gal4 UAS-Flp UAS>CD2,y^{+}>mCD8::GFP* single cell flip-out clones. **(G–I)** *L4^{0980}-Gal4* driving *UAS-mCD8::GFP*.**. (J–L)** *splitL4-Gal4* driving *UAS-mCD8::GFP*. **(B,E,H,K)** are magnifications of the boxed areas in **(A,D,G,J). (M)** *L4^{0987}-LexA* driving *LexAop-rCD2::GFP*. **(N)** *L4^{0987}-QF* driving *QUAS-mCD8::GFP*. **(O)** *L4^{0980}-QF* driving *QUAS-mCD8::GFP*. Scale bar: 50 μm in **(A–O)**, 5 μm in the inset panels in (**B**) and (**E**). See also Figure S2.

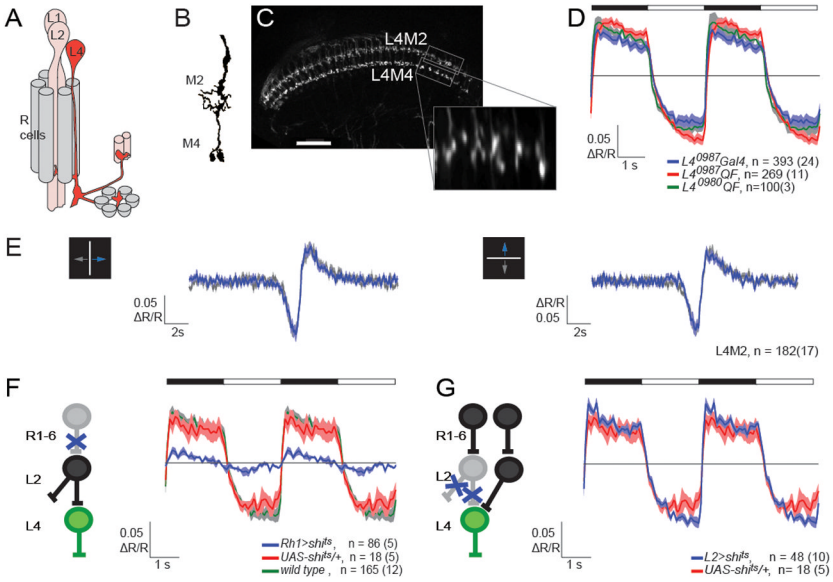

Figure 3. Physiological characterization of L4 reveals multiple inputs

(A) Schematics of a lamina cartridge. L2 receives input from R cells and synapses onto L4, which sends collateral projections into two neighboring cartridges. Modified from Strausfeld and Campos-Ortega (1973). **(B)** Illustration of the L4 arbor in the M2 and M4 layers of the medulla (modified from Fischbach and Dittrich, 1989). **(C)** Two-photon image of TN-XXL expression in L4 terminals. Boxed areas indicate regions used for imaging in M2 and M4. Scale bar: 30 μm. The inset represents such an ROI as an average time-series image after alignment. **(D)** Averaged responses (ΔR/R) of L4 axons in M2 to periodic full field flashes. The timing of light off and light on is depicted by the filled and open portions of the bar, respectively. Different binary expression systems were used as indicated. Shading denotes +/− 1 SEM. **(E)** Averaged response (ΔR/R) of L4 axons in M2 to an approximately 2.5° wide bright bar, moving at 10°/s either right and left (left panel) or up and down (right panel) on a dark background. **(F,G)** L4 responses to full field flashes were imaged using *L4^{0987}-QF QUAS-TN-XXL* while the either R1-R6 **(F)** or L2 neurons **(G)** were synaptically silenced. All flies were pre-incubated at 37°C. Sample sizes are indicated as number of cells(flies) imaged. See also Figure S3.

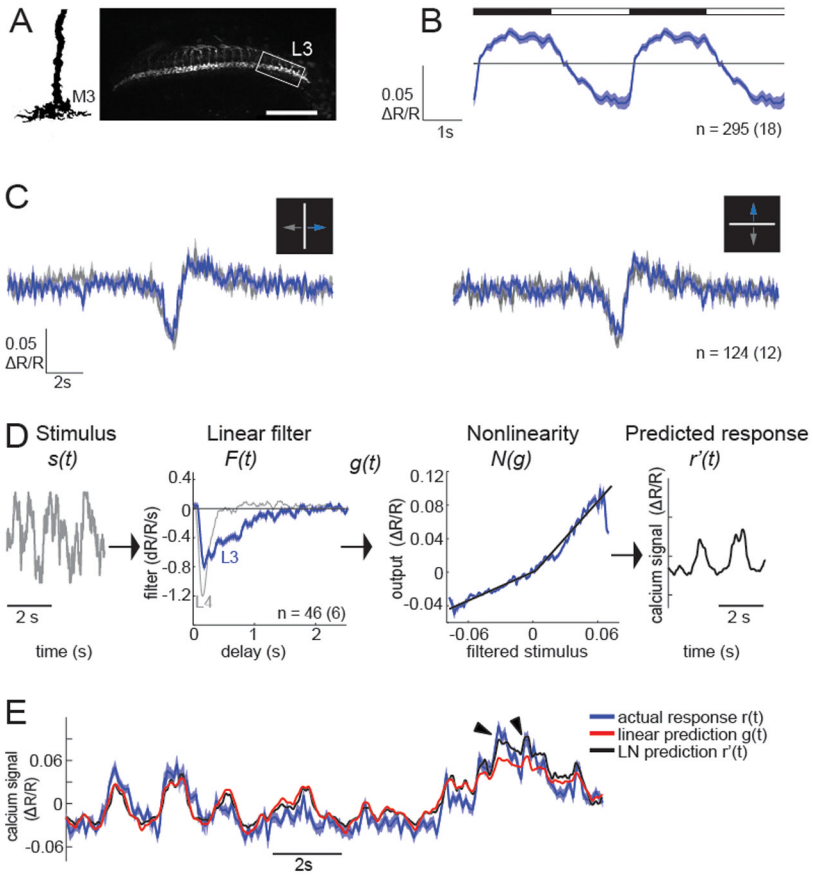

Figure 4. Calcium signals in L3 axons are sustained, and non-linear

(A) Illustration of the L3 arbor in the M3 layer of the medulla (modified from Fischbach and Dittrich, 1989). Two-photon image of TN-XXL expression in L3 axons. Scale bar: 30 μm. The box indicates a typical ROI. **(B)** Average responses (ΔR/R) of L3 to periodic full field flashes. The timing of lights off and lights on is depicted by the filled and open portions of the bar above the traces. **(C)** Average response (ΔR/R) to an approximately 2.5° wide bright bar, moving at 10°/s either horizontally (left panel) or vertically (right panel) on a dark background. **(D)** LN model based on responses to a gaussian stimulus: The stimulus waveform *s(t)* is passed through a linear temporal filter *F(t)* (blue), and the result *g(t)* is transformed by two linear fits (black) to a nonlinear function *N(g)* (blue) to obtain the predicted response $r'(t)$. For comparison, the linear filter of L4 is shown in gray. **(E)** Calcium response predicted by the linear filter or the full LN model compared to the actual calcium response (mean +/− 1 SEM). Arrowheads point to strong calcium responses that are better captured by the LN prediction. Sample sizes are indicated as number of cells(flies) imaged. See also Figure S4.

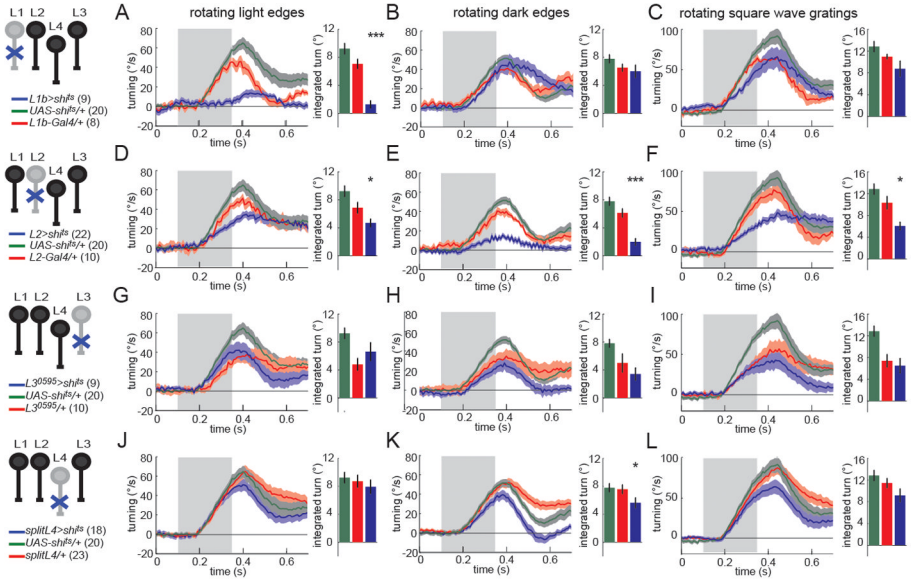

Figure 5. L3 and L4 are individually dispensable for responses to rotational motion

(A–L) Turning behavior in response to various rotational stimuli. Each panel shows the experimental *Gal4>shi^{ts}* condition (blue) as well as the corresponding *Gal4/+* (red) and *UAS-shi^{ts}/+* (green) controls. Shading denotes +/− 1 SEM. Genotypes and schematics are shown to the left. Number of flies run per genotype is indicated in parentheses. The bar plots next to each time trace show integrated responses over a 250 ms window beginning 80 ms after stimulus onset. *p<0.05, ***p<0.001, tested using two-tailed t-tests against both controls. Error bars denote +/− 1 SEM.

(A,D,G,J) Turning responses to rotating light edges. Multiple light bars appear on a dark background. One edge of each bar then expands in the same direction at 80°/s. **(B,E,H,K)** Turning responses to rotating dark edges. Multiple dark bars appear on a light background. One edge of each bar then expands in the same direction at 80°/s. **(C,F,I,L)** Turning responses to rotating square wave gratings with 40° spatial period and moving at a contrast frequency of 9 Hz. See also Figure S5.

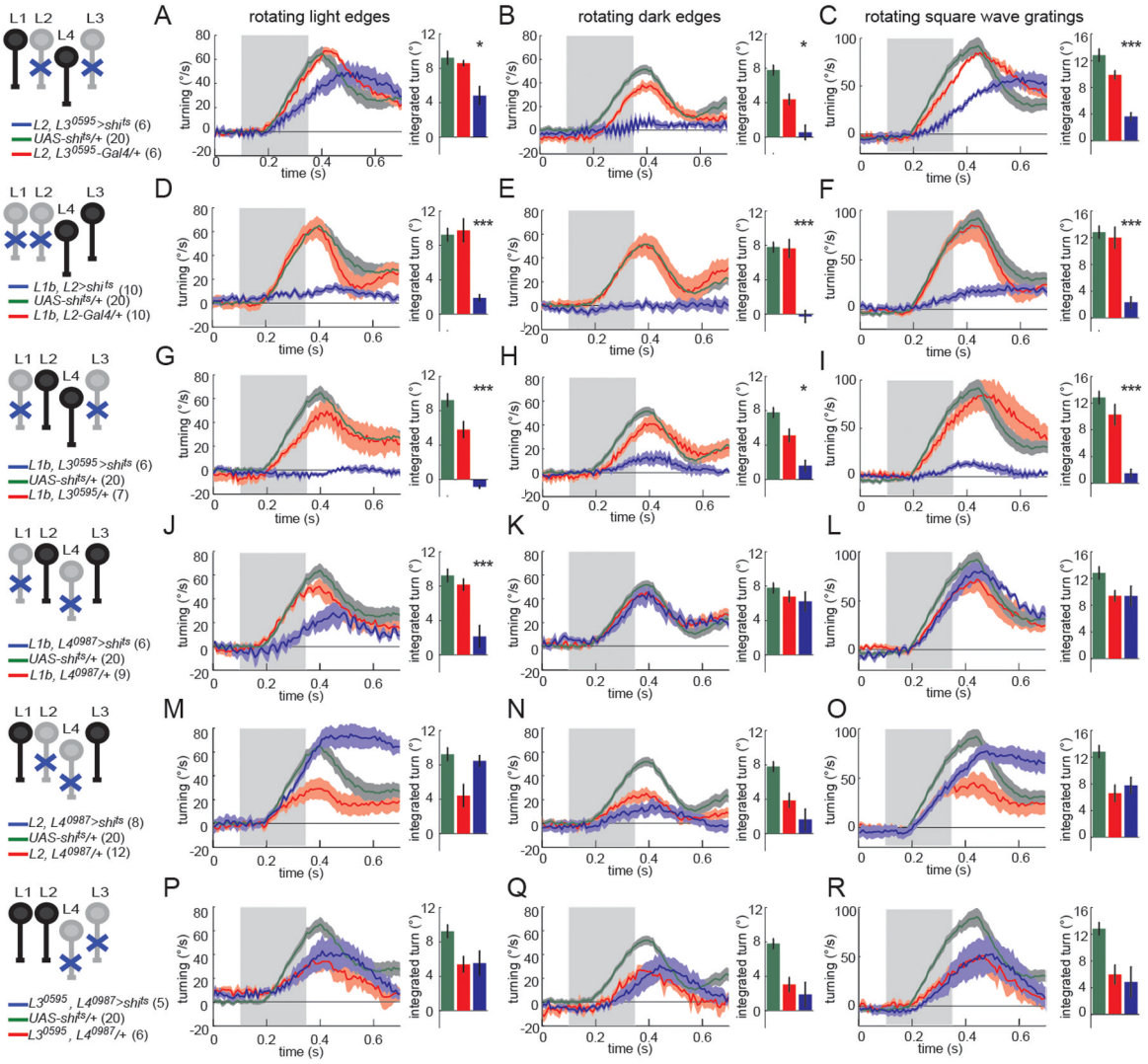

Figure 6. Circuits that compute responses to dark edge motion receive inputs from L1, L2 and L3

(A–R) Turning behavior in response to various rotational stimuli. Each panel shows the experimental *Gal4(1)+Gal4(2)>shi^{ts}* condition (blue) as well as the corresponding *Gal4(1)+Gal4(2)/+* (red) and *UAS-shi^{ts}/+* (green) controls. Shading denotes +/− 1 SEM. Genotypes and schematics are shown to the left. Number of flies run per genotype is indicated in parentheses. The bar plots next to each time trace show integrated responses over a 250 ms window beginning 80 ms after stimulus onset. *p<0.05, ***p<0.001, tested using two-tailed t-tests against both controls. Error bars denote +/− 1 SEM.

(A,D,G,J,M,P) Turning responses to rotating light edges. Multiple light bars appear on a dark background. One edge of each bar then expands in the same direction at 80°/s.

(B,E,H,K,N,Q) Turning responses to rotating dark edges. Multiple dark bars appear on a light background. One edge of each bar then expands in the same direction at 80°/s.

(C,F,I,L,O,R) Turning responses to rotating square wave gratings with 40° spatial period and moving at a contrast frequency of 9 Hz. See also Figure S6.

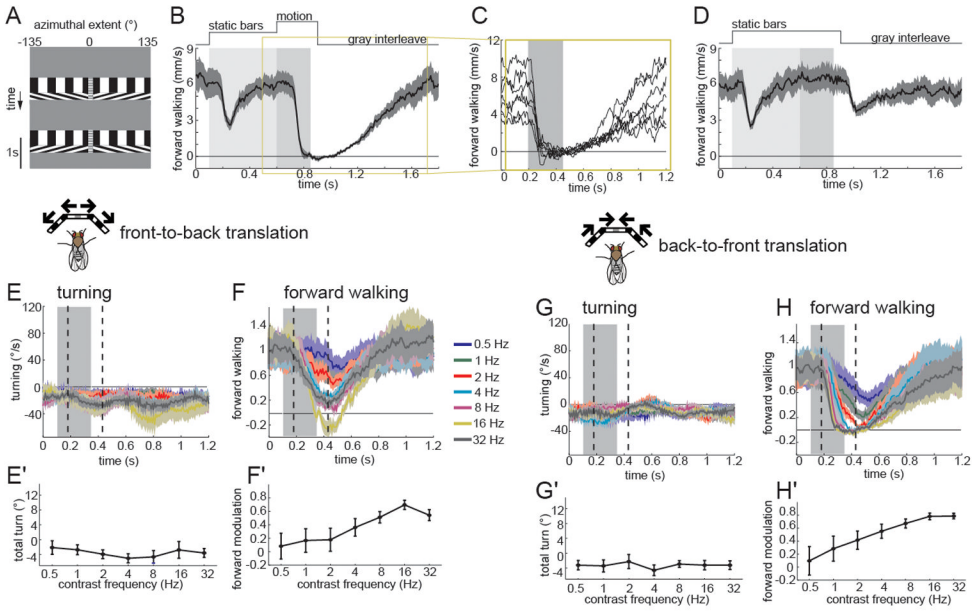

Figure 7. Visual motion can specifically modulate forward walking behavior

(A) x-t plot of the back-to-front (top) and front-to-back (bottom) translational motion stimulus used in Figures 7–9. Square-wave gratings with a 40° spatial period were projected on a virtual cylinder at 30% contrast. The stimulus consists of a 1 s gray interleave, followed by the appearance of the square wave grating which moves for 250 ms after a 500 ms delay between the appearance of the pattern and the onset of its movement. A 10° wide flickering stripe (30 Hz) marked the pole of expansion in front of the fly. **(B)** Top: Trial structure for translational stimuli. The region shaded light gray highlights the time during which static bars are displayed and the dark gray shaded area denotes the motion period. Bottom: Average forward walking response of *UAS-shi*^{ts}/+ control flies in response to a 6 Hz back-to-front translational stimulus. n=7 flies. Shading denotes +/− 1 SEM. **(C)** Mean responses of individual flies that contributed to the group average shown in the highlighted region of panel **(B). (D)** No motion control. A startle effect was observed caused by the appearance and disappearance of the square wave grating, but flies did not modulate their translation during the period in which motion is typically presented. **(E–H)** Average turning **(E, G)** and normalized forward walking **(F, H)** responses to front-to-back (**E, F**) and back-to-front **(G, H)** translational motion stimuli moving at the indicated contrast frequencies. The gray filled area denotes the stimulus presentation time. The two dashed lines indicate the time window over which the integrated response in panel E′-H′ is calculated. This window is 250 ms in duration, and begins 80 ms after stimulus onset. Shading denotes +/− 1 SEM. n=8 flies. Integrated turning response **(E′, G′)** and forward walking **(F′, H′)** of the traces shown in **(E–H)**. Error bars denote +/− 1 SEM. See also Figure S7.

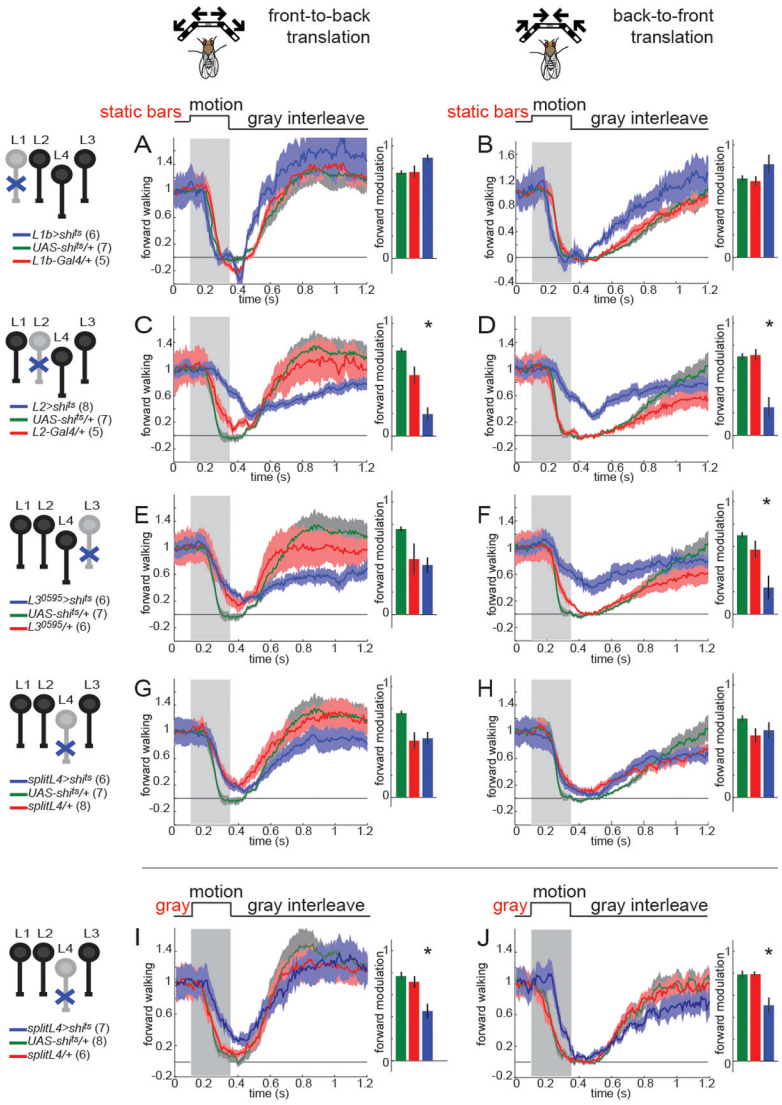

Figure 8. L2 and L3, but not L1 or L4 are required for modulation of forward walking behavior by translational motion stimuli

(A–J): Normalized average forward walking speed as a function of time for front-to-back motion (**A,C,E,G,I**) and back-to-front motion (**B,D,F,H,J**). In (**A–H**), moving square wave gratings were shown after a 500ms delay, in which the pattern appeared, but was stationary. In (**I,J**), the motion period started without a delay. The stimulus was presented at a contrast frequency of 6 Hz for all panels. Genotypes and schematics are shown to the left of each panel. Number of flies run per genotype is indicated in parentheses. Gray bar denotes the motion epoch. The *Gal4>shi^ts* experimental traces in which the indicated neuron is silenced are always displayed in blue, *UAS-shi^ts/+* controls in green and *Gal4/+* controls in red. The bar plots next to each time trace show integrated responses over a 250 ms window beginning 80 ms after stimulus onset. *p<0.05 tested using two-tailed t-tests against both controls. Shading around mean traces and error bars denote +/− 1 SEM. See also Figure S8.

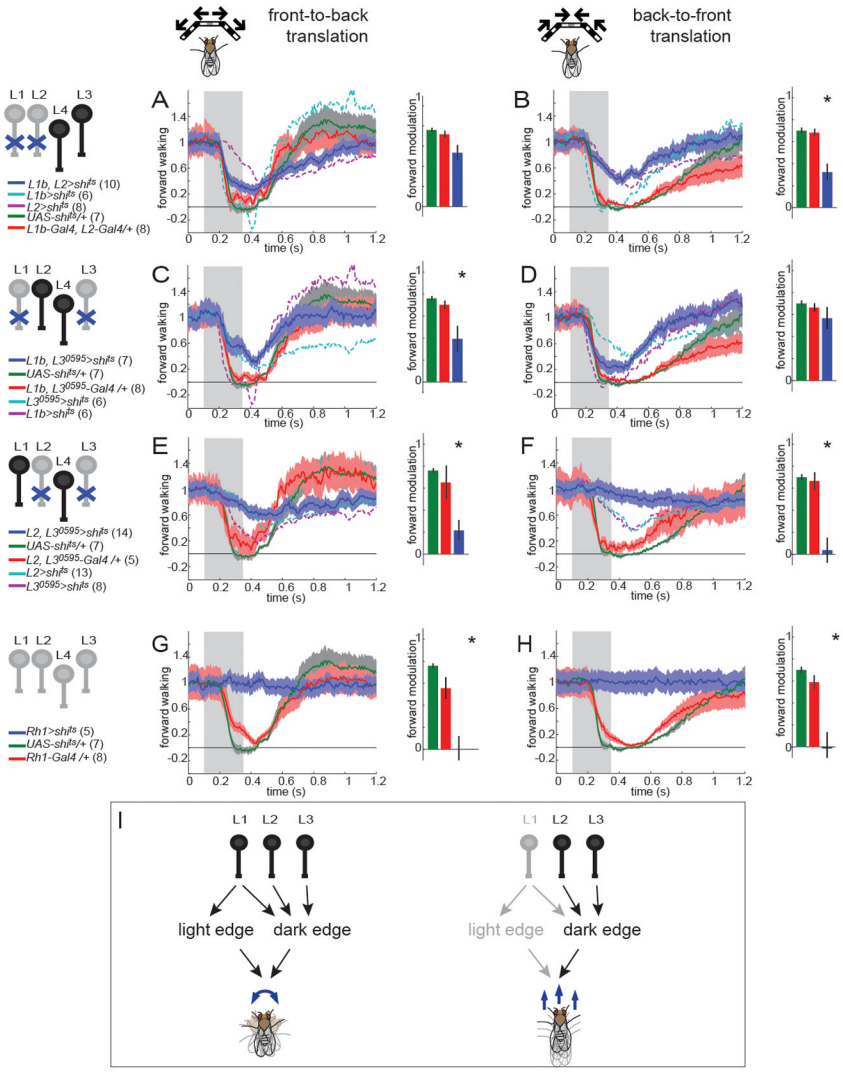

Figure 9. Responses to translational and rotational motion utilize different input architectures

(A–H): Normalized average forward walking speed for front-to-back **(A,C,E,G)** and back-to-front motion **(B,D,F,H)**. The stimulus was presented at a contrast frequency of 6 Hz for all panels. Genotypes and schematics are shown to the left. Number of flies run per genotype is indicated in parentheses. Gray bar denotes the motion epoch. The *Gal4(1)+Gal4(2)>shi^{ts}* experimental traces are always displayed in blue, *UAS-shi^{ts}/+* controls in green and *Gal4(1)+Gal4(2)/+* controls in red. Dashed lines (light blue and magenta) indicate the mean forward walking speed for the corresponding single silencing controls. The bar plots show integrated responses over a 250 ms window beginning 80 ms after stimulus onset. *p<0.05 tested using two-tailed t-tests against both controls. Shading around mean traces and error bars denote +/− 1 SEM. **(I)** A schematic summarizing how different combinations of input channels contribute to edge detection and modulate turning and forward walking behavior. See also Figure S9.